Backward K^-p elastic scattering and 0° $\Sigma^-\pi^+$ production

M. Alston-Garnjost, R. P. Hamilton, R. W. Kenney, D. L. Pollard,* and R. D. Tripp
Lawrence Berkeley Laboratory, University of California, Berkeley, California 94720

H. Nicholson
Mount Holyoke College, South Hadley, Massachusetts 01075

D. M. Lazarus
Brookhaven National Laboratory, Upton, New York 11973

(Received 24 September 1979)

In this paper we report measurements of the backward K^-p differential cross section at 49 momenta covering the momentum range 476–1084 MeV/c. The statistical precision achieved, typically 2.5%, is an order of magnitude better than previous measurements. The systematic errors for this reaction are about 1%. The differential cross section for the reaction $K^-p \to \Sigma^-\pi^+$ where the π^+ emerges at 0° has also been measured at 32 momenta with comparable improvement in precision over previous experiments. A partial-wave analysis of the $\bar{K}N$ channels including the new K^-p backward elastic data is presented.

I. INTRODUCTION

It has been demonstrated for the pion-nucleon system that the measurement of elastic scattering cross sections in the backward direction will often dramatically enhance the evidence for resonances.[1] Comparable experiments with the K^-p system had not been undertaken for the investigation of hyperon resonances because of much lower available K^- fluxes and certain other experimental difficulties inherent in the K^-p system.

To see why backward scattering is favorable for the observation of resonant effects, consider the partial-wave decomposition of the backward-scattering cross section. For a kaon scattering angle of 180°, the spin-flip amplitude is absent and the Legendre polynomials are $(-1)^l$, where l is the orbital angular momentum. Thus, the differential cross section I may be written as

$$I = \frac{1}{k^2}\left|\sum_{J,\pm}(-1)^l(J+\tfrac{1}{2})T_J^{\pm}\right|^2, \qquad (1)$$

where $T_J^{\pm}$ are the partial-wave amplitudes for the total angular momentum $J = l \pm \frac{1}{2}$ and k is the c.m. wave number. For the K^-p system, inelastic channels, which constitute nearly half of the total cross section, cause the scattering amplitudes $T_J^{\pm}$ to be predominantly positive imaginary. Hence, even- and odd-parity states tend to cancel in their contributions to backward scattering so that usually the background cross section is small. Furthermore, any resonant amplitude gives its maximum contribution in the backward (and forward) directions because its Legendre polynomial is unity at these angles. For these reasons a small resonant amplitude should reveal itself most prominently in the backward direction.

In recent years evidence has been presented for a number of new hyperon resonances. In particular, high-precision remeasurement of the K^-p and K^-d total cross sections by Carroll *et al.*[2] has given indications for six new resonances, all quite narrow and of low elasticity. On the other hand, our subsequent measurements of the total[3] and differential cross sections[4] for the charge-exchange reaction $K^-p \to \bar{K}^0n$ have shown no structure in this mass region which cannot be fitted adequately[5] with the older well-established resonances. As a complement to our charge-exchange work, we have undertaken a measurement of the backward elastic differential cross section with the aim of greatly improving the precision of the measurement, compared to extant data, in a situation favorable to the observation of narrow resonances, should they exist.

The statistical precision of previous backward-scattering data, derived almost exclusively from bubble-chamber experiments,[6-9] is quite poor. These data are exhibited in Fig. 1(a) and are seen to have widely varying errors, typically 5% to 45%, with an average uncertainty of about 25%. Electronic experiments[10,11] designed to improve upon bubble-chamber statistics have not succeeded because of inadequate K^- beams and, furthermore, for the very backward direction the requirement of two-body coincidence fails because the backward-scattered K^- usually stops in the hydrogen target. In order to circumvent this problem in our work, we have eliminated the requirement of a two-body coincidence. The elastically scattered protons emerging from the target in the forward direction were identified by momentum and time of flight, utilizing a focusing spectrom-

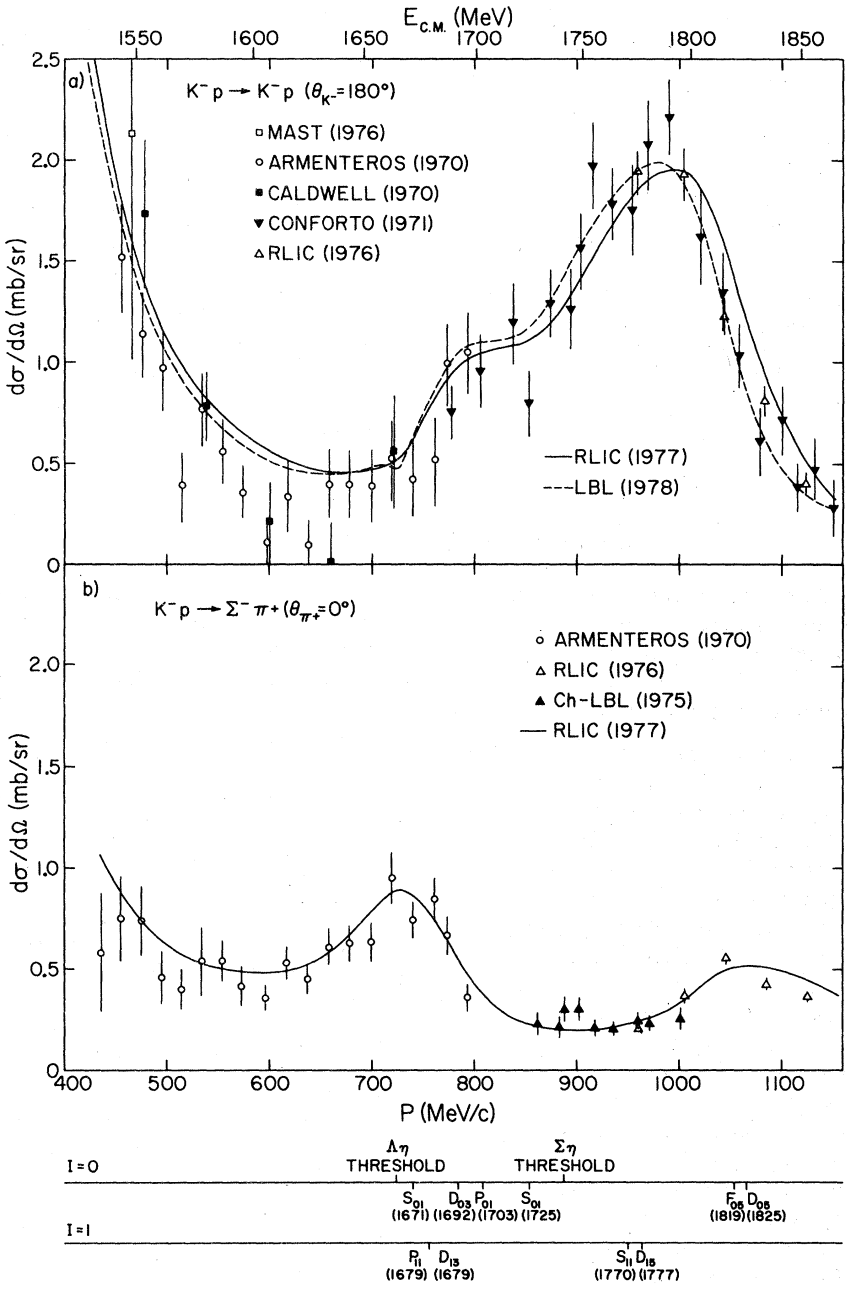

FIG. 1. Previous measurements: (a) Differential cross section for $K^-p \to K^-p$ at $\theta_{K^-}=180°$ (Refs. 6–9 and 25). (b) Differential cross section for $K^-p \to \Sigma^-\pi^+$ at $\theta_{\pi^+}=0°$ (Refs. 6, 8, and 12). The curves are the predictions of two recent partial-wave analyses (Refs. 5 and 17).

eter and a 45-channel hodoscope. The monoenergetic protons resulting from elastic events were clearly evident above a background of protons arising from hyperon decays. In this way we have improved by more than a factor of 10 on the statistical precision of the previously available backward-scattering cross sections.

The apparatus can be utilized unchanged to investigate other two-body reactions where one of the particles has a lifetime sufficiently long to pass through the spectrometer and reach the hodoscope. In practice, one is limited to particles of opposite sign to the beam because of contamination from the unscattered beam. Hence, we have also measured the differential cross section for the reaction $K^-p \to \Sigma^-\pi^+$, where the

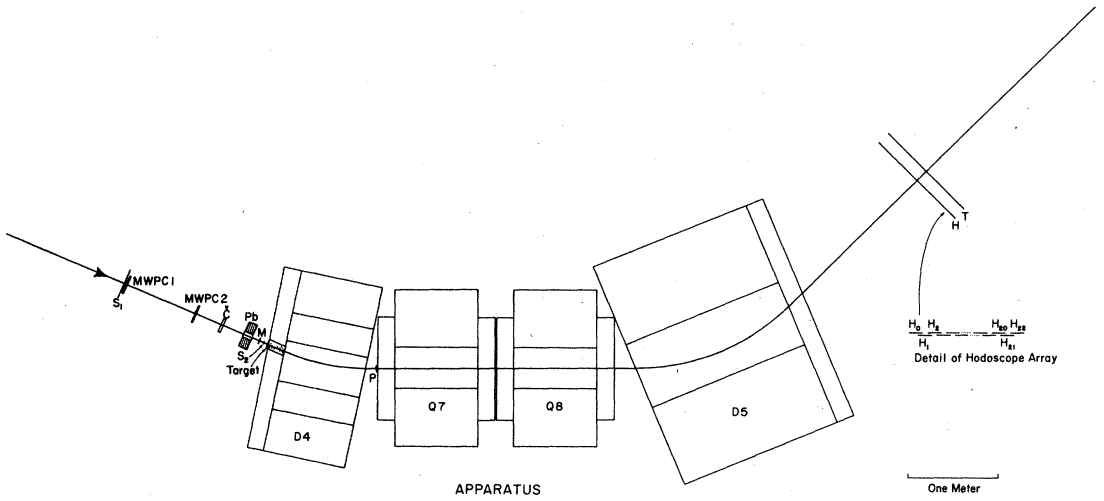

FIG. 2. The experimental apparatus.

π^+ emerges at 0°. Comparable improvement in statistics over previous bubble-chamber data[6,8,12] [Fig. 1(b)] has been achieved for this reaction.

II. EXPERIMENTAL ARRANGEMENT

The experimental arrangement (Fig. 2) consisted of a separated beam defined by three scintillation counters, a Čerenkov counter to identify kaons, and a liquid-hydrogen target. Downstream from the target a four-element spectrometer was placed on the 0° beam line. This spectrometer focused the 0° particles scattered out of the target onto the central $\frac{1}{3}$ of a hodoscope consisting of 23 vertical scintillators. The outer $\frac{2}{3}$ of the hodoscope was used for background determination. The flight time of the secondary was used to identify the particle as an aid in background suppression.

The beam used in the experiment was the momentum-recombined branch ($C4$) of the low-energy separated beam (LESB) at the Brookhaven National Laboratory Alternating Gradient Synchrotron (AGS).[13] For the discussion that follows refer to Tables I and II for the dimensions of the counters and the focal properties of the magnets.

The envelope of the incident beam was defined by three counters (S_1, M, and S_2). Counter S_1, an anticounter having an aperture for passage of the beam, was placed directly after the last beam-line magnet where it served to eliminate any halo of divergent particles around the beam. Counter M was the zero-time reference counter for the electronic logic, and counter S_2 defined the acceptable beam immediately upstream of the target. A pair of multiwire proportional chambers (MWPC's) was positioned downstream of the S_1 counter for use in beam tuning and for measuring accurately the horizontal image of the beam at the hydrogen target. The vertical image was measured by a removable hodoscope which consisted of five horizontal scintillators.

A Čerenkov counter ($\check{C}$)[3,14] with liquid or Plexiglas radiator was used to distinguish kaons from the pions and other particles in the beam. Although there were typically 10 times as many pions as kaons in the beam, using this counter we were able to reduce the misidentification of kaons in the beam to less than 1% at most beam momenta.

A lead collimator with an aperture for beam passage was placed between the Čerenkov counter

TABLE I. Dimensions of scintillation counters and spectrometer magnets.

Counter of collimator	Thickness (cm)	Width (cm)	Height (cm)
S_1 (aperture)	0.32	15.24	2.54
M	0.32	10.16	5.08
S_2	0.32	3.81	3.18
P	0.32	7.62	25.40
Final hodoscope (H)	0.32	59.69	30.48
Lead collimator (aperture)	10.16	10.16	5.08

TABLE II. Transformation matrix of spectrometer from target to focus. The vector, labeled x, θ_x, y, θ_y, $\Delta P/P$, is in units of cm, msr, and per cent.

−0.649	0	0	0	−2.19
−7.28	−1.54	0	0	0
0	0	−3.88	0	0
0	0	−3.50	−0.284	0
0	0	0	0	1

and the M counter. This collimator reduced the number of π's and μ's from the decay of back-scattered kaons, or π's from Σ^- decays, that could have entered the Čerenkov counter where they could have vetoed good beam kaons.

The liquid-hydrogen target was a cylindrical Mylar flask 20.96 cm long and 10 cm in diameter. The total thickness of all Mylar in the target structure upstream and downstream of the hydrogen was 0.292 and 0.191 mm, respectively. The pressure in the target when filled was 1.109 atm, and thus the density of the liquid parahydrogen was 0.07037 g/cm^3.[15]

Immediately following the target was an 18D36 dipole magnet (D_4), with a 25.4-cm gap.[16] This magnet swept away the unscattered beam and most of the unwanted particles at 0°. Downstream from this magnet was placed a pair of 18Q36 quadrupoles (Q_7 and Q_8) which focused the scattered beam through the last dipole magnet in the spectrometer, a 36D72 dipole magnet (D_5) gapped to 20.3 cm giving vertical and horizontal foci 50.8 and 152.4 cm, respectively, downstream from the dipole magnet. This final magnet enabled us to obtain a highly dispersed image of the target at the detector hodoscope (H). The momentum acceptance of the hodoscope ($\Delta p/p$) was about ±13% at all incident momenta.

The solid-angle acceptance of the spectrometer was defined primarily by a thin scintillation counter (P) 25.4 cm high and 7.62 cm wide placed in the scattered beam 140.36 cm from the target center giving an acceptance of 9.8 msr. The total acceptance was calculated by the Monte Carlo techniques discussed below.

The final hodoscope (H) consisted of 23 scintillators each 30.48 cm high and 3.8 cm wide. The counters were placed so that nearest neighbors overlapped as shown in Fig. 2, giving a hodoscope of 43 channels each 1.27 cm wide and 2 outer channels 2.54 cm wide. The image of the target formed at the hodoscope by the spectrometer was about 13 cm wide and 20 cm high centered on the hodoscope.

The time-of-flight (TOF) array (T) consisted of two counters each 59.7 cm long and 15.24 cm high placed immediately downstream of the hodoscope. Any particle accepted by the spectrometer that hit the hodoscope also hit one of these two timing counters. A third counter, of the same dimensions, was vertically centered on the junction of the two primary TOF counters and was used only for positional tagging. (The resulting combination of these three counters divided the vertical region of the hodoscope into four channels each 7.62 cm high.)

The total flight path for the TOF system was 8.5 m, and the inclusion of cuts on the particle TOF in the electronics resulted in a substantial reduction in the trigger rate due to unwanted particles from background reactions, especially when investigating the reaction $K^-p \to \Sigma^-\pi^+$.

A block diagram of the electronics is shown in Fig. 3. The beam envelope was defined by a coincidence (B) between the main timing counter (M) and (S_2), with the halo counter (S_1) in anti-coincidence. 90% of a separate signal from M was fed through a special dead-time circuit[14] that generated a signal if an acceptable beam particle had no neighbors closer than ±65 nsec in time. When this signal (DT) was put into coincidence with (B), the result was a rate-independent beam signal (BD). A kaon-coincidence signal (K) and a pion veto (π) from the Čerenkov counter were put into coincidence and veto, respectively, with (BD) at (BK). The possibility of good events vetoing themselves was much reduced for the reaction $K^-p \to K^-p$ by utilizing the pulse height in counter M. Decay products from backward-scattered kaons could have entered the Čerenkov counter to produce a "pion" veto signal, but rarely without the slow backward-scat-

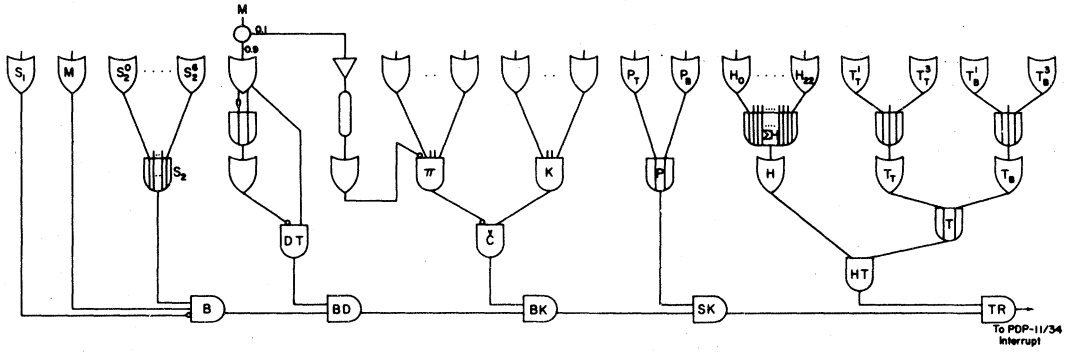

FIG. 3. System electronics. B = beam particle, BK = beam kaon, SK = scattered kaon, TR = Trigger (interrupt computer).

tered kaon having traversed the M counter. The double traversal of M gave a large pulse that was detected by a discriminator whose threshold was set at approximately 3.5 times the "minimum ionizing" pulse height. This discriminator's output was used to cancel the pion veto of the Čerenkov counter.

The coincidence of the Čerenkov counter ($\check{C}$) and the rate-independent beam signal (BD) became the kaon beam-definition signal (BK) used in the final cross-section calculation. The passage of an acceptable scattered particle through the spectrometer was defined by a coincidence (SK) between the beam-kaon signal (BK), and a signal from the P counter (P). All the signals from the hodoscope counters were fanned together and put into coincidence with a gate from the TOF counter system (T) at (HT). The final event trigger (TR) was determined by a coincidence of the (HT) signal and the scattered kaon signal (SK).

The data-acquisition system consisted of CAMAC interfaced to a PDP 11/34 computer. All the counters in the H and T hodoscopes were fed into CAMAC latches, most of the coincidences and many of the single counters were scaled, time of flights were recorded in CAMAC time-to-digital converters (TDC's) and pulse heights for the M counter and each of the TOF counters were recorded by CAMAC analog-to-digital converters (ADC's). When an event trigger (TR) occurred, an interrupt was fed to the PDP 11/34 and the event information was read into the computer. Between AGS pulses, the computer performed several minor checks and conversions on the raw data (e.g., converting latch bit patterns into hodoscope channel numbers) and then wrote the data onto magnetic tape for further off-line analysis. In addition, the computer accumulated the data on line and could display, on command, histograms of various quantities such as events per hodoscope channel or ADC or TDC distributions. This facility was very useful in the setup and debugging of the experiment and also for on-line monitoring of the experimental operation.

III. DATA ACQUISITION

At each momentum data were accumulated in a series of runs with the target full and empty. When the target was empty most of the triggers were caused by secondaries (proton or π^+) from K^- interactions upstream of the target, i.e., in the Čerenkov counter and counters M and S_2 (see Fig. 2). When the target was full, these background secondaries lost energy in the hydrogen in the target. To make their trajectories in the spectrometer the same in both cases, the spectrometer magnets were retuned for higher-momentum particles for empty runs so that we were able to make a direct target full-empty subtraction in each channel of the H hodoscope.

Histograms of the hodoscope distributions were made for target full and empty at each momentum. For target empty the distribution was normalized by a factor k_1, where k_1 = (number incident K^- target full)/(number incident K^- target empty). The distributions for $K^-p \to K^-p$ for $P_{K^-} = 1007$ MeV/c are shown in Fig. 4. In the region of the peak the normalized target-empty triggers were typically 15 to 20% of the target-full counts. The number of triggers in the data peak after the target-empty subtraction was approximately 600 at each of the low momenta and 6000 at high momenta. For the reaction $K^-p \to \Sigma^-\pi^+$, the hodoscope distributions were similar to those for $K^-p \to K^-p$ and the useful events ranged between approximately 250 and 2000.

IV. CALCULATION OF CROSS SECTION

The backward differential cross section was calculated from the expression

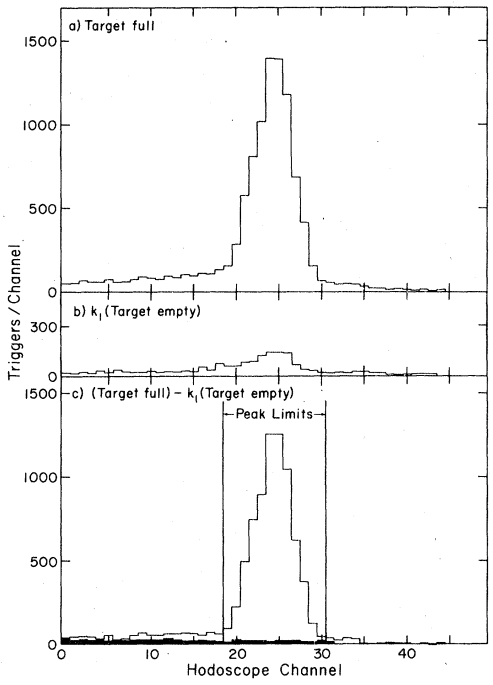

FIG. 4. Hodoscope distributions for $K^-p \to K^-p$ ($\theta_{K^-} = 180°$) for $p_{K^-} = 1007$ MeV/c. Low-momentum protons are on the left. (a) Target full. (b) (Target empty) $\times k_1$, where k_1 = (beam flux with target full)/(beam flux with target empty). (c) (Target full) $- k_1 \times$ (target empty). The black area is the background predicted by Monte Carlo calculations.

$$\frac{d\sigma}{d\Omega} = \frac{A}{\rho L N_0} \frac{1}{N_{BK}} \frac{d\Omega_{\text{lab}}}{d\Omega} \frac{1}{\Delta\Omega_{\text{lab}}} \left(\prod C_i\right)\left(F - \frac{k_1 M}{C_7'} - B\right), \tag{2}$$

where $A = 1.008$, the atomic weight of hydrogen; $\rho = 0.070$, the density of liquid parahydrogen under our target conditions after subtraction of the gas-filled–empty effect; L = target length measured along its cylindrical axis; N_0 = Avogadro's number; N_{BK} = the number of beam particles, electronically identified as kaons, that produced F counts when the target was full; $d\Omega_{\text{lab}}/d\Omega$ = the solid-angle transformation; $\Delta\Omega_{\text{lab}}$ = the laboratory solid angle of the P counter = 9.8 msr; M = the observed number of counts with target empty and for N_{BK}/k_1 incident kaons; B = the background discussed below. The various C_i contained in the product ΠC_i and C_7' are corrections that are approximately unity and are treated in detail in Sec. V.

The analysis of runs at each incident beam momentum began with the subtraction, channel by channel of the H hodoscope, of the renormalized target-empty counts from the counts observed with target full, i.e., data in Fig. 4(b) were subtracted from those in Fig. 4(a). From this difference spectrum upper and lower cuts were made as shown in Fig. 4(c). Care was taken to make these limits sufficiently wide to avoid loss of tails of the data peak and also to make the width of the peak smoothly momentum dependent. Our Monte Carlo model, which included multiple scattering in material downstream of the interaction point in the target, showed that these limits always included the full elastic peak of protons on the hodoscope from $K^- p \to K^- p$. For $\Sigma^- \pi^+$ all π^+'s and about $\frac{2}{3}$ of the μ's (from π decays) which hit the hodoscope were contained within the limits of the data peak. Those μ's falling outside the peak were mainly on the low momentum side.

A two-step evaluation of the background B involved a Monte Carlo calculation of other reactions, and a determination of a residual background. For $K^- p \to K^- p$, the Monte Carlo background calculation included reactions that yielded protons, from Λ or Σ decay, which entered the spectrometer and reached the hodoscope. They are in order of importance, $K^- p \to \Lambda\pi^0$, $\Lambda\pi\pi$, $\Sigma^+\pi^-$, $\Sigma^0\pi^0$, and $\Sigma\pi\pi$. The cross sections and angular distributions of the two-body final states were calculated from the phase-shift-analysis results of Gopal *et al.*[17] For the three-body states we assumed the isotropic production of $\Sigma(1385)\pi$ and $\Lambda(1520)\pi$, followed by the isotropic decay of the resonance. Results of the Monte Carlo were in the form of triggers versus hodoscope channel number at eleven beam momenta. An example, for 1007 MeV/c incident K^-, is shown in Fig. 5(a), normalized to the experimental beam flux (N_{BK}). The $\Lambda\pi^0$ reaction was dominant and the $\Sigma\pi\pi$ reaction contributed the least. The relative magnitudes of the others were dependent on momentum and channel number. Figure 4(c) also shows the sum of the separate Monte Carlo results as the black area. The difference between the two distributions in Fig. 4(c), namely, the Monte Carlo–background–subtracted data, is shown in Fig. 5(b). The tails that remain in Fig. 5(b) are evidence of a background we were never able to explain adequately. This additional background was subtracted by averaging its magnitude over several channels on the low-momentum side of the data peak and similarly on the high-momentum side. The additional background under the elastic peak was then assumed to be the average of the low- and high-momentum additional backgrounds. This unexplained background comprised about 4% of the events in the data peak at the higher momenta and was negligible at lower momenta. This described our best estimate of the additional background under the data peak. Accordingly

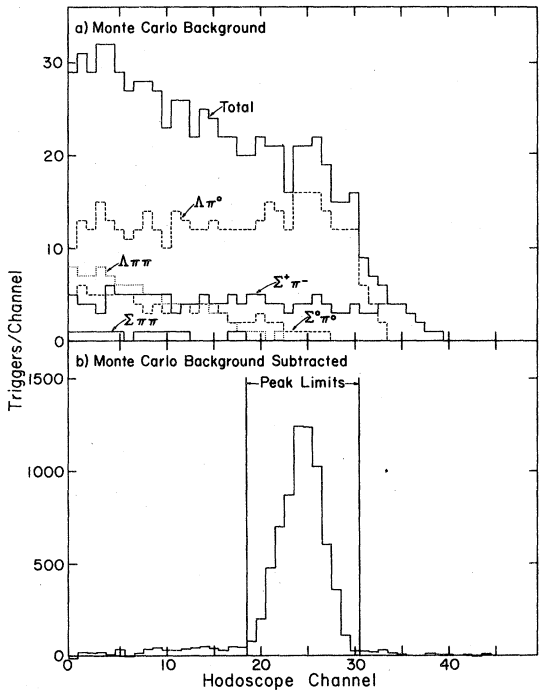

FIG. 5. Hodoscope distributions for $p_{K^-} = 1007$ MeV/c. (a) Monte Carlo–predicted background for reactions $\Lambda\pi^0$, $\Lambda\pi\pi$, $\Sigma^+\pi^-$, $\Sigma^0\pi^0$, and $\Sigma\pi\pi$ normalized to the experimental beam flux. (b) Monte Carlo–background-subtracted data, i.e., [data in Fig. 4(c)] − [data in Fig. 5(a)]. Note some additional background is still present. (See text, Sec. IV.)

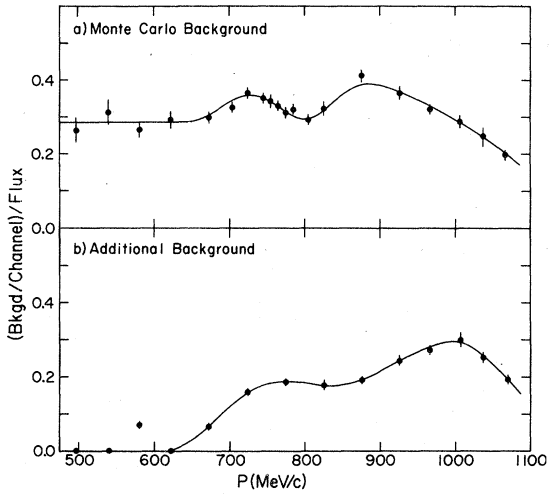

FIG. 6. Backgrounds per hodoscope channel for $K^-p \to K^-p$ ($\theta_{K^-} = 180°$) as a function of beam momentum normalized to a flux of 10^6 incident kaons. Statistics are those of the Monte Carlo calculations. (a) Background predicted by Monte Carlo calculations. (b) Additional background required to describe the observed hodoscope distributions.

these numbers were subtracted from the data in Fig. 5(b) to give our best estimate of the true hydrogen effect, apart from additional corrections that will be treated below. Monte Carlo evaluation of background followed by this subtractive process was carried out at eleven beam momenta spanning the momentum interval of the experiment. The Monte Carlo background and the additional background per channel for each momentum is shown in Fig. 6 for K^-p normalized to a beam flux (N_{BK}) of 10^6. Smooth curves were drawn through the points and these interpolated values were used in the detailed reduction of the data at each beam momentum. Up to this point C_7' [See Eq. (2)], whose value is very nearly unity, was ignored because its effect upon the evaluation of the residual background is masked by statistical fluctuations.

For $K^-p \to \Sigma^-\pi^+$ Monte Carlo calculations of the background caused by $K^-p \to \bar{K}^0 n$ followed by $K_S^0 \to \pi^+\pi^-$ were made at four beam momenta. Again there was an unexplained residual background of about 4%. Since the $K_S^0 \to \pi^+\pi^-$ background was distributed uniformly over the hodoscope it proved more convenient to estimate the total $K^-p \to \Sigma^-\pi^+$ background using the procedure described above for the $K^-p \to K^-p$ additional background rather than to compute Monte Carlo and additional backgrounds separately. This total background was estimated at 13 beam momenta and the results are shown in Fig. 7.

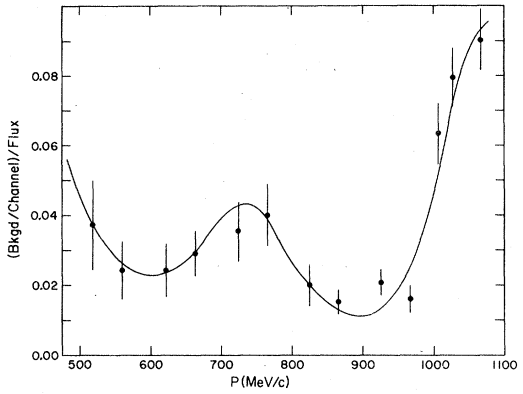

FIG. 7. Total background per hodoscope channel for $K^-p \to \Sigma^-\pi^+$ ($\theta_{\pi^+} = 0°$) as a function of beam momentum normalized to a flux of 10^6 incident kaons.

V. CORRECTIONS

Ten corrections to the observed raw cross section were applied in an effort to account for a number of small effects, none of which exceeded a few percent in magnitude. They are listed in Table III and their magnitudes are plotted in Fig. 8. These corrections are discussed in more detail in Ref. 18. All Monte Carlo corrections were found to be consistent with rough hand calculations of their values. The corrections were divided into two quite different classes. First there were the corrections to the beam flux and to the path length in the liquid-hydrogen target. The second class of corrections dealt with the loss of scattered secondary protons or π^+ between the liquid-hydrogen target and the hodoscope.

A. Background scattering in target (C_7')

Equation (2) singled out the correction factor C_7' from all others, it being required in the target-empty subtraction. All other correction factors were multiplicative. The factor C_7' accounted for the scattering in hydrogen of empty-target secondaries, nearly all of which were produced upstream of the liquid-hydrogen target. Thus, the counting rate observed when the target was empty was not a true representation of the corresponding background component of the counting rate when the target was full because those particles in the background coming from upstream of the hydrogen target could be scattered in the filled hydrogen target and might not reach the hodoscope. Values of the cross sections from Refs. 19 and 20 were used.

TABLE III. Corrections to observed cross section.

		C_i	δC_i		
A. K^- beam-intensity and path-length corrections					
C_1	Beam contamination (π, μ, e)	1.0001–1.021	±0.001		
C_2	Decays of beam K^- between Čerenkov and S_2 counter	1.0098	±0.0002		
C_3	Interactions of beam K^- in counter S_2	1.0041	±0.0005		
C_4	Decays of beam K^- between counter S_2 and downstream end of target	1.0204–1.0469	±0.0001		
C_5	Interactions of beam K^- in target	1.0148–1.0225	±0.0001		
C_6	Target length (end profile averaged over beam distribution)	1.0230	±0.0005		
B. Losses of secondaries					
		$K^-p \to K^-p$		$K^-p \to \Sigma^-\pi^+$	
		C_i	δC_i	C_i	δC_i
C_7	Absorption in hydrogen, acceptance of spectrometer	1.041–1.060	±0.002	1.033–1.067	±0.002
C_7'	Absorption of secondaries in hydrogen (difference for target full vs empty)	1.020–1.037	±0.0004	1.013–1.052	±0.0015
C_8	π^+ decay ($\Sigma^-\pi^+$ only)	1.000		1.120–1.299	±0.002
C_9	Backward K^- vetoes (K^-p only)	1.0002–1.0011	±0.0004		
	Backward Σ^- vetoes ($\Sigma^-\pi^+$ only)			1.000	
C_{10}	Absorption in P counter and air column in spectrometer	1.014	±0.002	1.016	±0.002

B. Corrections to beam flux and K^- track length in hydrogen [Fig. 8(a)]

1. Beam contamination (C_1)

The correction C_1 dealt with beam contamination. The charged-particle beam that was accepted in the experiment consisted principally of kaons with a measured contamination of pions. The magnitude of the level of the contamination is shown in Fig. 8(a).

2. Kaon decay between Čerenkov and S_2 counters (C_2)

The factor C_2 corrected the incident beam intensity for decay of K^- mesons between the Čerenkov counter, where kaons were identified, and the scintillator S_2. The electronics did not distinguish kaons from those charged secondaries that arose downstream of the Čereknov counter; accordingly, the observed incident beam flux was corrected downward to account for contamination.

A simple Monte Carlo program was used to follow these charged decay products and to evaluate the ratio Δ/N of false electronic kaon signatures Δ in a total of N incident particles accepted by the system.

3. Kaon interaction in counter S_2 (C_3)

The incident beam intensity was corrected for kaon interactions in the final scintillation counter S_2. Particles from these interactions gave rise to an electronic signal in S_2 that was indistinguishable from that recorded by a kaon that entered the target. This was not necessarily the case for interactions of beam kaons in the counter M preceding S_2 because of the requirement that a simultaneous count also be recorded in S_2. The solid angle for interaction products counting in S_2 reduced the M-interaction correction to a negligible level. The total absorption cross section for kaon-scintillator interactions was estimated to be 271 mb.[21-23]

4. Kaon decay from S_2 through hydrogen target (C_4)

The correction C_4 accounted for decays of beam kaons in the interval from the final counter S_2 to the downstream window of the hydrogen target.

5. Kaon interactions in target hydrogen (C_5)

The factor C_5 corrected the measured incident beam flux for interactions in the hydrogen[24] by averaging this loss over the length of the target.

6. Mean length of hydrogen target (C_6)

The factor C_6 accounted for the mean track length in the hydrogen target being somewhat less than the maximum axial-target dimension because of the convex windows of the hydrogen vessel and the horizontal and vertical extent of the beam spot. The spatial distributions of the beam were measured by a wire chamber array

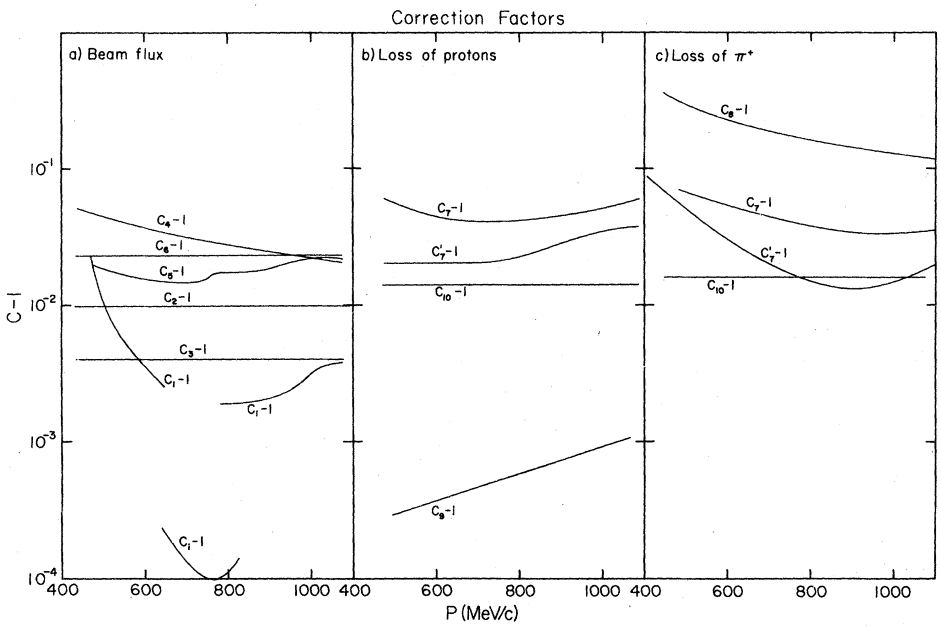

FIG. 8. Multiplicative correction factors discussed in Sec. V. (a) Corrections to beam flux and target length. (b) Corrections for loss of secondary protons. (c) Corrections for loss of secondary π^+.

and a removable hodoscope located in the incident beam. Observed beam distributions at the upstream and the downstream windows of the hydrogen vessel were averaged over the convex windows and the mean target length computed. The result was essentially independent of momentum because the beam geometry was nearly independent of momentum.

C. Loss of secondaries

The second class of corrections dealt with the loss of forward secondaries that arises from interactions in the counters, hydrogen target, and air in the spectrometer. The values are shown in Figs. 8(b) and 8(c).

1. Geometric acceptance of spectrometer and loss of secondaries due to scatters in the target (C_7)

In order to maximize the counting rate, the P counter, which defined the solid angle, was made slightly larger than the geometric acceptance of the spectrometer. As a result some secondaries were lost due to scraping at the spectrometer magnet apertures. This was particularly true at low momenta.

To calculate this correction, the Monte Carlo began by generating $K^-p \to K^-p$ or $K^-p \to \Sigma^-\pi^+$ interactions in the target, taking into account the attenuation of the K^- beam in hydrogen so that interactions were somewhat more likely toward the upstream end of the target. A check was then made to see if the proton or pion interacted with the hydrogen in the target along its trajectory. Particles that did interact were assumed to be lost. Surviving secondaries that went through the P counter were followed through the rest of the spectrometer. For calculating this correction, pions were assumed to be stable. C_7 is thus the ratio of the number of "P" counts to the number of counts in the hodoscope peak.

2. π^+ decays in $K^-p \to \Sigma^-\pi^+$ (C_8)

For the reaction $K^-p \to \Sigma^-\pi^+$ our apparatus counted both π^+'s, and μ^+'s from π^+ decays. However, not all of the μ^+'s reached the hodoscope due to scraping at the magnet apertures. Also, some μ^+'s hit the hodoscope outside the limits imposed on the data peak. In a second version of the Monte Carlo program pions were allowed to decay along the spectrometer flight path and the muon's trajectory through the spectrometer was followed to see where it hit the hodoscope. Approximately 30% of the muons from π^+ decays were found to hit the hodoscope under the data peak. C_8 was then the ratio of "stable" pions that would reach the hodoscope to the number of pions and muons that reached the hodoscope within the limits of the data peak when the pions were allowed to decay. Figure 8 shows the results of a least-squares fit to the Monte Carlo results for C_8.

3. Self-veto (C_9)

The lead collimator and the high-threshold M counter veto circuit were designed to reduce the vetoes of beam particles that produced backscattered K^-'s. Such K^-'s or their decay products, pions and muons, could, in principle, reach the Čerenkov counter and veto good $K^-p \to K^-p$ events by producing a false "pion" signal and thereby lead to a cross-section value that was too small. Our Monte Carlo calculations showed that no K^-'s and only a few pions and muons from these backscattered events could produce such vetoes. For the reaction $K^-p \to \Sigma^-\pi^+$ a calculation showed that π^- from the decay of the slow Σ^- could only reach the Čerenkov counter through the aperture in the lead wall and had insufficient velocity to produce a "pion" signal. Thus, C_9 is unity for this reaction. C_9 was the factor by which the experimentally measured number of events must be scaled upward to account for these losses.

4. Interactions of secondaries in the P counter and the air column in the spectrometer (C_{10})

Secondary particles could be absorbed by the P counter or the air column. To calculate this

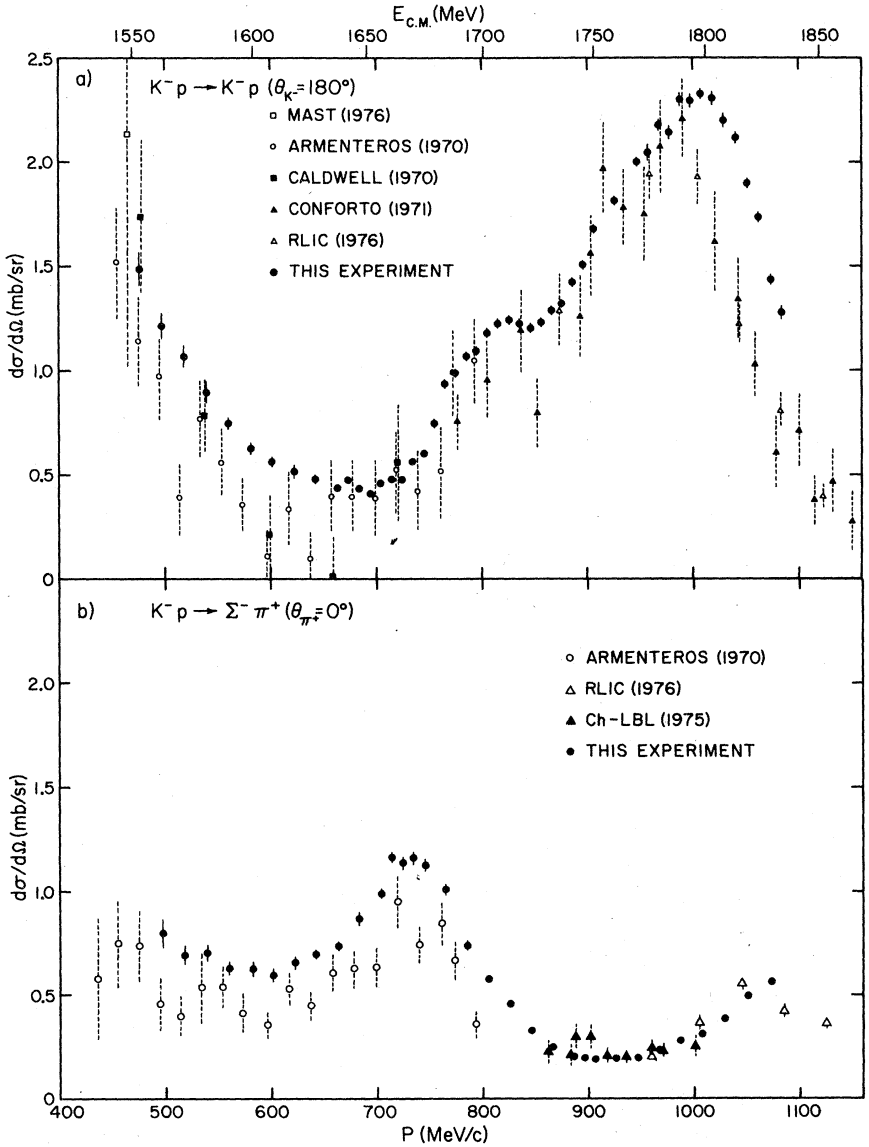

FIG. 9. Comparison between the results of this experiment and previous data (Refs. 6–9, 12, and 25). (a) Differential cross section for $K^-p \to K^-p$ at $\theta_K = 180°$. (b) Differential cross section for $K^-p \to \Sigma^-\pi^+$ at $\theta_{\pi^+} = 0°$.

correction we assumed that the absorption cross sections for p and π^+ in scintillator and air were constant over the momentum range of the experiment. The cross section for scintillator was estimated by scaling the p ^{12}C and π^+ ^{12}C cross sections giving values of 240 and 270 mb for protons and π^+, respectively. For air, cross-section values of 260 mb for p ^{14}N and 300 mb for π^+ ^{14}N were used.[22]

VI. RESULTS

The results of this experiment are shown in Figs. 9 and 10 and tabulated in Tables IV and V as a function of mean interaction momentum. The errors are statistical only and are typically about 2.5% for $K^-p \to K^-p$ (180°) and 4% for $K^-p \to \Sigma^-\pi^+$ (0°). This is an improvement in precision of more than a factor 10 over previous

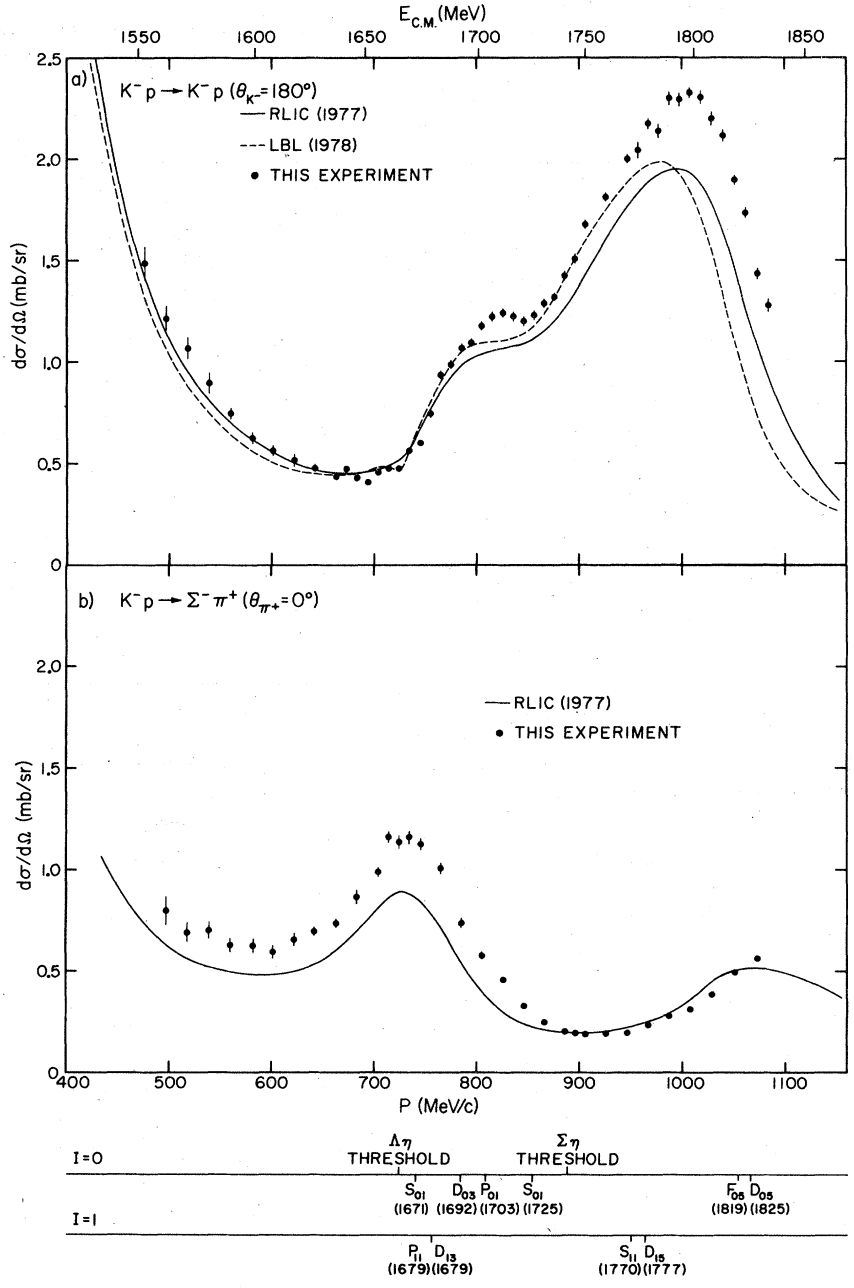

FIG. 10. Comparison between the results of this experiment and two recent partial-wave analyses (Refs. 5 and 17).

TABLE IV. Differential cross section in the c.m. at 180° ($\langle\cos\theta\rangle=-0.995$) for the elastic scattering $K^-p\to K^-p$ as a function of incident K^- beam momentum (P_{K^-}).

P_{K^-} (MeV/c)	$\frac{d\sigma}{d\Omega}(180°)$ (mb/sr)	P_{K^-} (MeV/c)	$\frac{d\sigma}{d\Omega}(180°)$ (mb/sr)
476	1.487 ± 0.085	826	1.240 ± 0.021
497	1.211 ± 0.067	836	1.220 ± 0.022
518	1.068 ± 0.057	846	1.197 ± 0.025
539	0.895 ± 0.051	856	1.229 ± 0.023
560	0.745 ± 0.031	866	1.289 ± 0.023
581	0.626 ± 0.030	876	1.319 ± 0.022
601	0.566 ± 0.029	886	1.424 ± 0.024
622	0.513 ± 0.030	896	1.507 ± 0.026
642	0.477 ± 0.019	906	1.677 ± 0.020
663	0.433 ± 0.016	926	1.811 ± 0.024
673	0.472 ± 0.013	947	2.000 ± 0.022
683	0.429 ± 0.015	957	2.044 ± 0.045
694	0.408 ± 0.015	967	2.178 ± 0.024
704	0.457 ± 0.012	977	2.140 ± 0.036
714	0.474 ± 0.013	987	2.300 ± 0.034
724	0.472 ± 0.011	997	2.295 ± 0.037
734	0.560 ± 0.014	1007	2.329 ± 0.023
745	0.599 ± 0.015	1018	2.305 ± 0.034
755	0.746 ± 0.019	1029	2.200 ± 0.035
765	0.932 ± 0.020	1040	2.117 ± 0.032
775	0.982 ± 0.021	1051	1.898 ± 0.025
785	1.063 ± 0.024	1062	1.738 ± 0.028
795	1.090 ± 0.021	1073	1.435 ± 0.026
805	1.176 ± 0.017	1084	1.279 ± 0.034
815	1.221 ± 0.023		

data. The magnitude of the systematic uncertainty is dominated by the uncertainty in the background which is estimated to be about 14% for backward elastic and varies between 30% at low momenta and 10% at high momenta for $\Sigma^-\pi^+$. This leads to an uncertainty in the cross sections of 0.5 to 1.0% for K^-p and 0.8 to 1.7% for $\Sigma^-\pi^+$. In addition, errors on the correction factors lead to a total uncertainty in the overall normalization of 0.8 to 1.2% for the K^-p backward elastic and 1.0 to 1.8% for the $\Sigma^-\pi^+$ (0°) cross sections, respectively.

Comparison of our K^-p backward elastic results with previous data[6-9,25] shows only fair agreement

TABLE V. Differential cross section in the c.m. for the reaction $K^-p\to\Sigma^-\pi^+$ for $\theta_\pi=0°$ ($\langle\cos\theta\rangle=0.996$) as a function of incident K^- momentum (P_{K^-}).

P_{K^-} (MeV/c)	$\frac{d\sigma}{d\Omega}(0°)$ (mb/sr)	P_{K^-} (MeV/c)	$\frac{d\sigma}{d\Omega}(0°)$ (mb/sr)
497	0.798 ± 0.071	785	0.738 ± 0.025
518	0.689 ± 0.050	805	0.577 ± 0.019
539	0.701 ± 0.044	826	0.456 ± 0.011
560	0.628 ± 0.037	846	0.329 ± 0.011
581	0.624 ± 0.036	866	0.248 ± 0.010
601	0.597 ± 0.033	886	0.200 ± 0.012
622	0.653 ± 0.034	896	0.194 ± 0.010
642	0.693 ± 0.022	906	0.188 ± 0.009
663	0.736 ± 0.023	926	0.191 ± 0.008
683	0.865 ± 0.038	947	0.193 ± 0.009
704	0.988 ± 0.026	967	0.234 ± 0.011
714	1.160 ± 0.029	987	0.279 ± 0.011
724	1.136 ± 0.033	1007	0.310 ± 0.015
734	1.160 ± 0.034	1029	0.385 ± 0.016
745	1.121 ± 0.031	1051	0.494 ± 0.016
765	1.007 ± 0.029	1073	0.561 ± 0.016

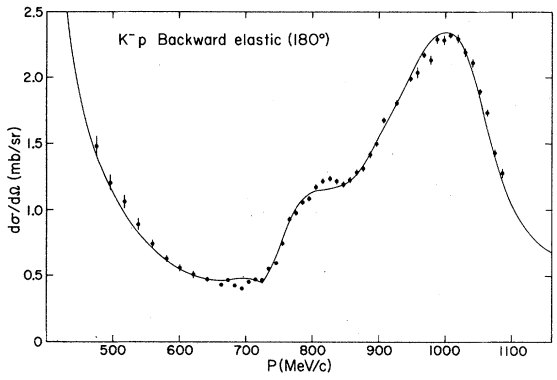

FIG. 11. The best PWA fit to our backward elastic scattering cross section without a new $D_{13}(1708)$ resonance.

with those experiments [Fig. 9(a)] and good agreement with partial-wave analyses (PWA)[5,17] up to 800 MeV/c incident momentum [Fig. 10(a)]. We can offer no explanation for the differences between the previous experiments and both our new data and the predictions of PWA. Above this momentum a bump in this cross section centered at about 830 MeV/c is seen which has not been observed before and is not predicted by recent partial-wave analyses.[5,17] Agreement between our data and both PWA predictions and previous data is good from 880 to 990 MeV/c. Above 990 MeV/c our new results are significantly higher than previous data and earlier PWA fits.

For the reaction $K^-p \to \Sigma^-\pi^+$ (0°) our results agree well with both previous data[6,8,12] and PWA

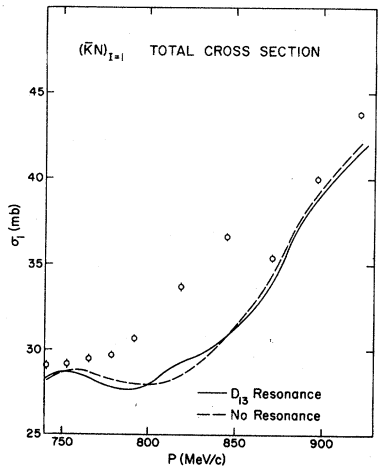

FIG. 12. The $I=1$ $\bar{K}N$ total cross section vs laboratory K^- momentum. The data points are from Carroll *et al.* with their quoted errors indicated. In the PWA we have enlarged these errors by about a factor of 5 to ±3%. The solid and dashed lines are best fits of the PWA to all K^-p data with and without a new D_{13} resonance. See Sec. VII of text.

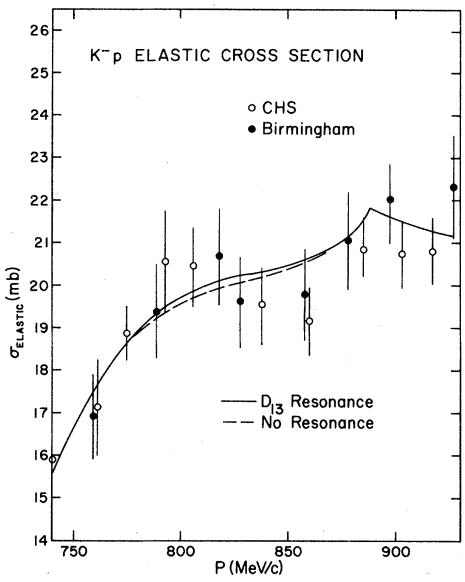

FIG. 13. The integrated K^-p elastic cross section as measured by bubble-chamber (Refs. 6, 7) (CHS) and counter (Ref. 11) (Birmingham) experiments. The cusp in the PWA curves is a result of the $\Sigma^0\eta$ threshold.

predictions[17] for the incident K^- momenta above 860 MeV/c. Below this momentum our results are significantly higher although the general features are similar, i.e., an enhancement at about 720 MeV/c and a broad valley near 600 MeV/c.

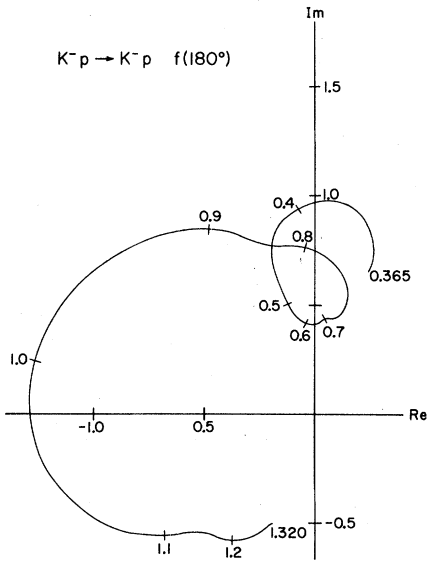

FIG. 14. A plot of the trajectory of the backward elastic scattering amplitude in the complex plane as a function of momentum. The amplitude is a result of the best PWA fit to all K^-p data without a D_{13} resonance near 825 MeV/c. Ticks indicate K^- laboratory momentum in GeV/c.

VII. PARTIAL-WAVE ANALYSIS (PWA)

These new backward elastic differential cross sections were introduced into our previously reported PWA of the elastic and charge-exchange channels with the following results (see Fig. 11). The significantly larger cross sections in the vicinity of 1000 MeV/c were easily accommodated in the revised PWA without altering the good fit below 800 MeV/c. This was accomplished through slightly enlarging some background amplitudes in the higher partial waves—those whose centrifugal barriers make them inconsequential at lower momenta. However, the relatively narrow enhancement in the region of 825 MeV/c remained difficult to fit (see Fig. 12). Even the introduction of an *ad hoc* resonance using a variety of spin-parity assumptions for the resonance did not adequately reproduce the bump and at the same time yield a χ^2 minimum for the fit of all data included in the analysis.

It should be noted that it was precisely in the region between 770 and 870 MeV/c where our previous fit[5] to the total $I=1$ cross sections was very poor and where these total cross sections indicated a structure. It was this structure which prompted Carroll *et al.*[2] to claim an $I=1$ resonance at a mass of 1715 MeV (833 MeV/c) with a width of 10 MeV and a height of 7 mb [corresponding to $(J+\frac{1}{2})x=0.30$]. An expanded view of the $I=1$ total cross section along with curves to be discussed later is exhibited in Fig. 12. In addition to these data, the integrated elastic cross sections as measured by two experiments[6,7,11] hint of structure in this region despite poor statistics, as can be seen in Fig. 13.

Either parity assignment can be considered for the resonance depending on whether one regards our structure as a bump at 825 MeV/c or a depression at 845 MeV/c, i.e., whether the interference between the small resonance and the dominant background amplitude at 180° is constructive or destructive. The trajectory of this background amplitude in the complex plane as a function of momentum as derived from our PWA is shown in Fig. 14. For the momentum region in question the amplitude is mostly positive

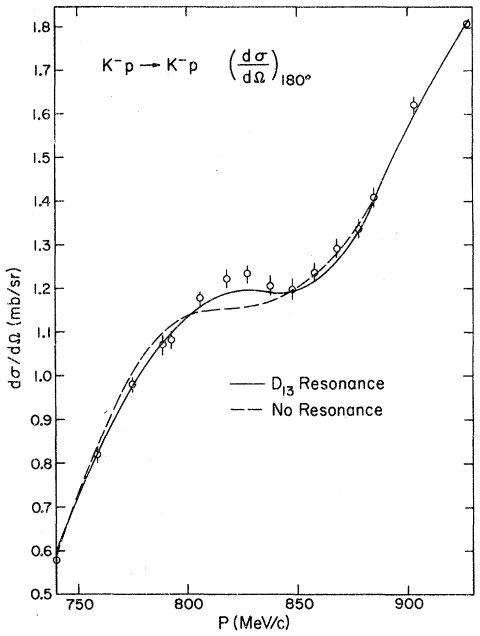

FIG. 15. The best PWA fit to our backward elastic scattering cross sections with and without a D_{13} resonance. The data points shown are those used in the PWA. They are interpolations of the actual data to momenta acceptable to the PWA program.

imaginary. Since the contribution of a resonance to backward scattering has a sign of $(-1)^I$, a resonance in an even angular momentum state would lead to a bump at resonance and an odd angular momentum state to a dip. Since the quoted mass of the structure seen by Carroll *et al.*[2] lies squarely in between, either possibility is admissible. We have assumed both hypotheses in our fits. To a certain approximation, our fits to these structures should be insensitive to the spin of the resonance since both the bump in the total cross section and the bump we observe in 180° scattering (arising primarily from interference between a small resonance and a large background) should be proportional to $(J+\frac{1}{2})x$, where the elasticity x is unknown. [See Eq. (1), where $T_J^{\pm}$ is proportional to x.]

Of the three J^P assumptions tried (S_{11}, P_{11}, D_{13}, where the notation is $L_{I,2J}$), the last yielded the

TABLE VI. Resonance parameters from this PWA and from the experiment of Carroll *et al.*

	Momentum (MeV/c)	Mass (MeV)	Width (MeV)	$(J+\frac{1}{2})x$
This experiment (D_{13} resonance)	818	1708	27	0.10
Carroll *et al.*	833	1715	10	0.30

lowest χ^2. It was, however, only marginally better than no resonance at all [$\chi^2(D_{13}$ resonance) = 2993, χ^2(no resonance) = 3017 with a total of 1652 data points and about 88 parameters]. The best-fit parameters for the resonance are compared to those of Carroll *et al.* in Table VI. Fits are shown with and without a resonance to our 180° elastic scattering data in Fig. 15, the integrated elastic cross sections (Fig. 13), and the $I = 1$ total cross sections (Fig. 12). Although none of the structures seen in these data is adequately fit, the most glaring disagreement lies with the $I = 1$ total cross sections. The PWA persistently refuses to follow these cross sections while at the same time fitting all other data included in the PWA. Neither are the $I = 0$ total cross sections well fit, although the K^-p total cross section, which shows very little structure, is adequately followed.

VIII. CONCLUSION

It is our conclusion from these experiments and from this PWA that the many structures found by Carroll *et al.* in their isospin-decomposed cross sections cannot be reconciled through PWA with the other K^-p interaction data. It would be highly desirable to repeat these total-cross-section measurements with the higher-intensity K^- beams and more suitable apparatus now available.

ACKNOWLEDGMENTS

We are grateful to the Brookhaven AGS staff for their generous assistance and hospitality and to T. Kycia for the loan of the Čerenkov counter. We also thank T. Daly and M. Long for technical assistance throughout the experiment. This work was supported by the High Energy Physics Division of the U. S. Department of Energy under Contracts Nos. W-7405-ENG-48, ER-78-S-02-4831, and EY-76-C-02-0016. One of us (H. N.) would like to thank the Faculty Grants Committee of Mt. Holyoke College and the University of Massachusetts Computer Center for financial support.

---

*Present address: Stanford Linear Accelerator Center, Stanford University, Stanford, California 94305.

[1]See, for example, W. Kormanyos *et al.*, Phys. Rev. Lett. 16, 709 (1966); E. Rothschild *et al.*, Phys. Rev. D 5, 499 (1972); W. F. Baker *et al.*, Phys. Rev. Lett. 32, 251 (1974).
[2]A. S. Carroll *et al.*, Phys. Rev. Lett. 37, 806 (1976).
[3]M. Alston-Garnjost *et al.*, Phys. Rev. D 17, 2216 (1978).
[4]M. Alston-Garnjost *et al.*, Phys. Rev. D 17, 2226 (1978).
[5]M. Alston-Garnjost *et al.*, Phys. Rev. D 18, 182 (1978).
[6]R. Armenteros *et al.*, Nucl. Phys. B21, 15 (1970); *ibid.* B8, 233 (1968).
[7]B. Conforto *et al.*, Nucl. Phys. B34, 41 (1971).
[8]B. Conforto *et al.*, Nucl. Phys. B105, 189 (1976).
[9]P. K. Caldwell *et al.*, Phys. Rev. D 2, 1 (1970).
[10]W. R. Holley *et al.*, Phys. Rev. 154, 1273 (1967).
[11]G. J. Adams *et al.*, Nucl. Phys. B96, 54 (1975).
[12]M. Jones *et al.*, Nucl. Phys. B90, 349 (1975).
[13]J. Fox, BNL Accelerator Dept. Notes No. 7, 1967 and No. 20, 1968 (unpublished).
[14]D. Pollard, thesis, Lawrence Berkeley Laboratory Report No. LBL-5522, 1976 (unpublished).
[15]R. J. Tapper, Report No. NIRL/R/95 (unpublished).
[16]AGS Experimenters Guide, Brookhaven National Laboratory, 1965 (unpublished).
[17]G. P. Gopal *et al.*, Nucl. Phys. B119, 362 (1977).
[18]R. Hamilton, thesis, Lawrence Berkeley Laboratory Report No. LBL-8969, 1979 (unpublished).
[19]E. Bracci *et al.*, CERN Report No. CERN/HERA 73-1, 1973 (unpublished).
[20]E. Bracci *et al.*, CERN Report No. CERN/HERA 72-1, 1972 (unpublished).
[21]R. J. Abrams *et al.*, Phys. Rev. D 4, 3235 (1971).
[22]V. S. Barashenkov *et al.*, Fortschr. Phys. 17, 683 (1969).
[23]The value for the K^--scintillator cross section 271 mb was estimated by scaling the K^--^{12}C cross section for density and by the ratio of mean absorption lengths in carbon and scintillator. The K^--^{12}C diffraction cross section was subtracted before scaling.
[24]E. Bracci *et al.*, CERN Report No. CERN/HERA 72-2, 1972 (unpublished).
[25]T. S. Mast *et al.*, Phys. Rev. D 14, 13 (1976).